

MEDICAL RADIOLOGY

Diagnostic Imaging

Editors:

A. L. Baert, Leuven
M. Knauth, Göttingen
K. Sartor, Heidelberg

S. O. Schoenberg · O. Dietrich · M. F. Reiser (Eds.)

Parallel Imaging in Clinical MR Applications

With Contributions by

E. Adalsteinsson · M. Aksoy · D. Atkinson · R. Bammer · P. G. Batchelor · T. Benner
M. Bock · J. W. Casselman · O. Dietrich · R. Duensing · R. Eibel · M. Essig
C. Fink · J. P. Finn · B. Fischer · M. A. Griswold · K. A. Herrmann · R. M. Hoogeveen
A. Huber · P. Kellman · H. Kramer · K.-F. Kreisner · D. J. Larkman · T. Leiner
C. Liu · C. A. McKenzie · H. J. Michaely · K. Nael · S. Nagle · K. Nikolaou · M. Nittka
N. Oesingmann · S. B. Reeder · W. Reith · A. Reykowski · J. Rieger · B. Romaneehsen
G. P. Schmidt · S. O. Schoenberg · B. Stieltjes · L. L. Wald · R. Wang · A. M. Wallnoefer
V. J. Wedeen · O. Wieben · G. Wiggins · B. J. Wintersperger · C. J. Zech

Foreword by

A. L. Baert

With 389 Figures in 774 Separate Illustrations, 137 in Color and 37 Tables

PD Dr. med. STEFAN O. SCHOENBERG
Dr. rer. nat. OLAF DIETRICH
Prof. Dr. med. Dr. h.c. MAXIMILIAN F. REISER
Department of Clinical Radiology
University Hospitals – Grosshadern
Ludwig Maximilian University of Munich
Marchioninistrasse 15
81377 Munich
Germany

MEDICAL RADIOLOGY · Diagnostic Imaging and Radiation Oncology
Series Editors: A. L. Baert · L. W. Brady · H.-P. Heilmann · M. Knauth · M. Molls · K. Sartor
Continuation of Handbuch der medizinischen Radiologie
Encyclopedia of Medical Radiology

Library of Congress Control Number: 2006925090

ISBN 3-540-23102-1 Springer Berlin Heidelberg New York
ISBN 978-3-540-23102-8 Springer Berlin Heidelberg New York

This work is subject to copyright. All rights are reserved, whether the whole or part of the material is concerned, specifically the rights of translation, reprinting, reuse of illustrations, recitations, broadcasting, reproduction on microfilm or in any other way, and storage in data banks. Duplication of this publication or parts thereof is permitted only under the provisions of the German Copyright Law of September 9, 1965, in its current version, and permission for use must always be obtained from Springer-Verlag. Violations are liable for prosecution under the German Copyright Law.

Springer is part of Springer Science+Business Media

<http://www.springer.com>

© Springer-Verlag Berlin Heidelberg 2007

Printed in Germany

The use of general descriptive names, trademarks, etc. in this publication does not imply, even in the absence of a specific statement, that such names are exempt from the relevant protective laws and regulations and therefore free for general use.

Product liability: The publishers cannot guarantee the accuracy of any information about dosage and application contained in this book. In every case the user must check such information by consulting the relevant literature.

Medical Editor: Dr. Ute Heilmann, Heidelberg

Desk Editor: Ursula N. Davis, Heidelberg

Production Editor: Kurt Teichmann, Mauer

Cover-Design and Typesetting: Verlagsservice Teichmann, Mauer

Printed on acid-free paper – 21/3151xq – 5 4 3 2 1 0

Foreword

The parallel imaging technique is a major technical development in MRI with a broad spectrum of clinical applications in various organs and organ systems of the human body.

This book is the first compilation to offer a comprehensive and detailed overview of the advantages and drawbacks of parallel imaging in clinical practice. It also provides a detailed description of the fundamental basic principles of this new method.

The editors of this book are internationally renowned experts in the field of MRI. Many contributions originate from the department of radiology at the Grosshadern University Hospital in Munich which, under the guidance of Prof. Dr. M. F. Reiser, has a long-standing reputation of excellence and leadership in cutting edge technology for medical imaging. Besides this group, other eminent European and overseas radiologists with outstanding knowledge and experience in new MR technology have contributed various chapters to this book.

I am very much indebted to the editors and the authors for their outstanding contributions resulting in this superb volume.

While I recommend this book to certified radiologists and radiologists in training, many other clinical disciplines involved in MR imaging will also benefit from the knowledge it offers.

I am convinced that this work will meet with great interest among our readership and that it will enjoy the same success as many other volumes previously published in our series Medical Radiology.

Leuven

ALBERT L. BAERT

Preface

Magnetic resonance imaging (MRI) has the substantial advantage over other imaging modalities that assessment of morphology can be combined with evaluation of function and metabolism. Due to the lack of exposure to radiation or iodinated contrast agents, imaging can be multiply repeated and extended to the entire body within a single MRI scan. However, in the past this appealing comprehensive approach was highly restricted due to limitations in speed and spatial resolution of the acquisitions.

Accelerating MRI has been one of the key incentives that resulted in the enormous technical progress of MRI we have witnessed during the last two decades. While early milestones in the history of accelerated MRI were fairly general improvements such as the introduction of fast gradient-echo or turbo-spin-echo pulse sequences and of the partial-Fourier approach in the mid-1980s, subsequent developments became more and more specific and limited to certain applications. These include in particular techniques such as key-hole imaging or echo sharing that were especially designed for fast dynamic MRI applicable only with a small number of very specific pulse sequences and imaging protocols.

Parallel imaging was also motivated by the desire to accelerate MRI when it was proposed in the second half of the 1990s. In contrast to many other techniques, however, it soon turned out to provide extraordinary advantages in virtually all areas of MRI, and thus, became one of the most important technical advances in current MRI technology. This was possible since parallel imaging can be applied to practically all types of pulse sequences and imaging protocols, ranging from high-resolution morphological imaging over various functional imaging techniques to ultra-fast dynamic MRI. In addition to substantially accelerated imaging, parallel MRI has been found to increase robustness of MR examinations and to reduce blurring of single-shot acquisitions as well as susceptibility and motion artifacts.

The major challenge for the successful implementation of parallel imaging in clinical routine was the introduction of multi-channel MRI technology which initially limited its widespread use. The key hardware requirement for parallel imaging is the capability to receive data in parallel from several independent coil elements. Some MRI systems had already provided this ability when parallel imaging became generally known and since then the number of receiver channels has been substantially increased from year to year. Thus, parallel imaging can now be clinically used at the vast majority of clinical and research sites.

This book, written by leading experts world-wide, aims to provide an in-depth introduction to parallel-imaging techniques and, in particular, to the application of parallel imaging in clinical MRI. It will provide readers with a broader understanding of the fundamental principles of parallel imaging and of the advantages and disadvantages

of specific MR protocols in clinical applications in all parts of the body at 1.5 and 3 Tesla. The first part of the book explains relevant MRI physics and techniques, detailing the various parallel-imaging reconstruction algorithms, pulse-sequence design for parallel imaging, as well as hardware considerations. Special emphasis was put on communicating these technical principles in a practical and coherent way attractive for physicists and physicians, radiological technicians, and researchers.

The second part presents detailed, ready-to-use clinical protocols for morphologic, angiographic, and functional MR imaging, with special emphasis on problem-solving strategies for assessment of cardiovascular and oncological diseases. Due to the introduction of new scanner platforms, these protocols are also extended from imaging of individual organs to disease-specific evaluation of the entire body. In addition, detailed information is provided on cutting-edge techniques such as diffusion-tensor imaging, oxygen-enhanced lung imaging, and MRA with blood-pool contrast agents.

We would like to thank Albert L. Baert as the responsible editor of the series “Medical Radiology – Diagnostic Imaging”, for his immediate endorsement of this book. We would also gratefully acknowledge the Springer publishers who enthusiastically supported us during the preparation of this book.

Munich

STEFAN O. SCHOENBERG
OLAF DIETRICH
MAXIMILIAN F. REISER

Contents

Part I: Basic Principles of Parallel-Imaging Techniques	1
1 MRI from k-Space to Parallel Imaging OLAF DIETRICH	3
2 Basic Reconstruction Algorithms for Parallel Imaging MARK A. GRISWOLD	19
3 The g-Factor and Coil Design DAVID J. LARKMAN	37
4 Measurement of Signal-to-Noise Ratio and Parallel Imaging SCOTT B. REEDER	49
5 Special Applications of Parallel Imaging DAVID ATKINSON	63
6 Parallel-Imaging Reconstruction of Arbitrary k-Space-Sampling Data ROLAND BAMMER, CHUNLEI LIU, and MURAT AKSOY	71
7 Complementary Techniques for Accelerated Imaging OLIVER WIEBEN	91
Part II: Sequence Design for (Auto-Calibrated) Parallel Imaging	105
8 Measurement of Coil Sensitivity Profiles MATHIAS NITTKA	107
9 Conventional Spin-Echo and Gradient-Echo Pulse Sequences OLAF DIETRICH	113
10 Single-Shot Pulse Sequences OLAF DIETRICH	119
11 Fast Sequences for Dynamic and Time-Resolved Imaging MICHAEL BOCK	127
12 The Development of TSENSE PETER KELLMAN	141

Part III: Technical Implementation in Clinical MRI 153

13 Design of Dedicated MRI Systems for Parallel Imaging
ARNE REYKOWSKI 155

14 Dedicated Coil Systems from Head to Toe
RANDY DUENSING 161

15 Design of Parallel-Imaging Protocols
STEFAN O. SCHOENBERG and OLAF DIETRICH 169

16 General Advantages of Parallel Imaging
OLAF DIETRICH 173

17 Limitations of Parallel Imaging
OLAF DIETRICH 177

Part IV: Clinical Applications: Imaging of Morphology 181

18 High-Resolution Imaging of the Brain
ROLAND BAMMER and SCOTT NAGLE 183

19 High-Resolution Imaging of the Skull Base and Larynx
JAN W. CASSELMAN 199

20 Lung Imaging
ROGER EIBEL 209

21 Liver Imaging
CHRISTOPH J. ZECH 219

22 High-Resolution Imaging of the Biliary Tree and the Pancreas
ASTRID M. WALLNOEFER, CHRISTOPH J. ZECH, and KARIN A. HERRMANN. 223

23 Parallel Imaging in Inflammatory Bowel Disease
KARIN A. HERRMANN. 247

24 Musculoskeletal Imaging: Knee and Shoulder
BERND ROMANEHSEN and KARL-FRIEDRICH KREITNER 255

25 Advanced Methods of Fat Suppression and Parallel Imaging
SCOTT B. REEDER and CHARLES A. MCKENZIE. 269

Part V: Clinical Applications: Angiography 283

26 MRA of Brain Vessels
ROMHILD M. HOOGEVEEN 285

27	MRA of the Carotid Arteries HENRIK J. MICHAELY and KAMBIZ NAEL	291
28	MRA of the Pulmonary Circulation KAMBIZ NAEL and J. PAUL FINN	307
29	MRA of the Renal Arteries STEFAN O. SCHOENBERG and JOHANNES RIEGER	319
30	Peripheral MR Angiography TIM LEINER	329
31	Pediatric Congenital Cardiovascular Disease STEFAN O. SCHOENBERG and CHRISTIAN FINK	349
32	High-Resolution Whole-Body MRA KONSTANTIN NIKOLAOU	355
Part VI: Clinical Applications: Function		369
33	Imaging of CNS Diffusion and Perfusion MARCO ESSIG, BRAM STIELTJES, and WOLFGANG REITH	371
34	Diffusion Tensor Imaging of the Brain THOMAS BENNER, RUOPENG WANG, and VAN J. WEDEEN	379
35	Imaging of Cardiac Function BERND J. WINTERSPERGER	393
36	Imaging of Cardiac Perfusion ARMIN HUBER	407
37	Imaging of Pulmonary Perfusion CHRISTIAN FINK	417
38	Oxygen-Enhanced Imaging of the Lung OLAF DIETRICH	429
39	Imaging of Renal Perfusion HENRIK J. MICHAELY and NIELS OESINGMANN	441
Part VII: Comprehensive Protocols		449
40	Cardiovascular Screening HARALD KRAMER	451
41	Tumor Staging GERWIN P. SCHMIDT	461

42 Imaging of Bronchial Carcinoma
STEFAN O. SCHOENBERG, CHRISTIAN FINK, and BASTIAN FISCHER 471

43 Imaging of Pulmonary Hypertension
KONSTANTIN NIKOLAOU and ARMIN HUBER 481

Part VIII: Future Developments 495

44 New Coil Systems for Highly Parallel MR Acquisition Strategies
LAWRENCE L. WALD and GRAHAM WIGGINS 497

45 Parallel-Excitation Techniques for Ultra-High-Field MRI
LAWRENCE L. WALD and ELFAR ADALSTEINSSON 511

46 Future Software Developments
PHILIP G. BATCHELOR 523

47 Future Imaging Protocols
STEFAN O. SCHOENBERG and OLAF DIETRICH 533

Subject Index 543

List of Contributors 557

The Development of TSENSE

PETER KELLMAN

CONTENTS

12.1	TSENSE Method	141
12.1.1	Background	141
12.1.2	Basic Concepts	141
12.1.3	Combined Spatial and Temporal Filtering	143
12.1.4	k-space Undersampling and Temporal Spectra	143
12.1.5	2D TSENSE	146
12.2	Application Examples	146
12.2.1	Cardiac Segmented Cine 2D Imaging	146
12.2.2	Real-Time Cardiac 2D Imaging	147
12.2.3	Contrast-Enhanced First-Pass Perfusion	147
12.2.4	Cardiac Cine 3D Imaging	149
12.3	Discussion	151
	References	152

12.1 TSENSE Method

12.1.1 Background

In dynamic imaging applications, temporal filtering and parallel imaging (spatial sensitivity encoding) may be combined to exploit the spatio-temporal correlation in the MR signals. In parallel imaging, the differences in spatial sensitivity of multiple receiver coils may be exploited using SENSE (PRUESSMANN et al. 1999) or SMASH (SODICKSON and MANNING 1997) techniques to eliminate the aliased component that results from undersampling k-space (for details see

Chap. 2). In dynamic imaging, temporal correlations may be exploited by using temporal interpolation methods such as view sharing (HU and PARRISH 1994), sliding window reconstruction, (D'ARCY et al. 2002) or, more generally, UNFOLD filtering (MADORE et al. 1999). These methods may be combined to achieve either higher acceleration factors (KELLMAN and McVEIGH 2000) or to improve suppression of alias artefacts (KELLMAN et al. 2001). The incorporation of temporal processing with image domain parallel imaging is referred to as TSENSE. The combination may also be used to realize auto-calibrating parallel imaging for greater robustness since auto-calibrating methods are less sensitive to subject motion (KELLMAN et al. 2001). Auto-calibrating TSENSE produces full spatial resolution coil sensitivity estimates for computing unmixing coefficients and, furthermore, does not require additional central scan lines which reduce the effective acceleration factor.

A number of new parallel imaging methods have incorporated the TSENSE strategy to exploit spatio-temporal correlations, such as k-t SENSE (TSAO et al. 2003) and UNFOLD-SENSE (MADORE 2004; MADORE 2002), and Auto-SENSE (KOSTLER et al. 2003). A method for generalized phased-array ghost elimination (PAGE) (KELLMAN and McVEIGH 2001; KELLMAN 2006) that uses parallel imaging to cancel ghosts arising from a variety of mechanisms uses the TSENSE method for auto-calibration. The TGRAPPA method is an extension of this technique to k-space domain parallel imaging (BREUER et al. 2005). The TSENSE methods may also be applied to non-Cartesian k-space acquisition such as radial or interleaved spiral (NEZAFAT et al. 2005).

12.1.2 Basic Concepts

A number of different methods have been demonstrated which increase the speed of MR acquisition by decreasing the number of sequential phase encodes

P. KELLMAN, PhD
Laboratory of Cardiac Energetics, National Institutes of Health/NHLBI, NIH Building 10/B1D-416, 10 Center Drive, msc-1061, Bethesda, MD 20892-1061, USA

through undersampling. Undersampling causes aliasing which results in a mixture of the desired image and wrap artefacts. Parallel imaging is one approach to undersampled image reconstruction. The mixture of desired image and alias artefacts may be separated using parallel imaging as shown in Fig. 12.1, in which the input images for individual coils have been reconstructed to a full FOV with wrap by zero-filling the undersampled k-space data. The individual coil images are then weighted and summed (pixelwise) with a phased-array combiner to cancel the wrap. The phased-array combiner coefficients are calculated based on in vivo estimates of the coil sensitivities by solving the inverse problem which maximizes the image SNR subject to a constraint of nulling the alias artefacts, the so-called SENSE method (see also Chapter 2; PRUESSMANN et al. 1999). In general, the noise level will vary across the FOV and may have hot spots due ill-conditioning of the parallel imaging solution. The noise amplification is also referred to as the g-factor and is discussed in detail in Chapter 3 (PRUESSMANN et al. 1999). Residual alias artefacts may also result due to errors in the sensitivity maps.

Another approach to undersampled image reconstruction for dynamic imaging uses temporal filtering (interpolation) to exploit inherent frame-to-frame correlation in dynamic imaging. The basic idea of interpolation is to compute additional time frames using a weighted sum of neighboring measurements

to gain a higher temporal sampling rate. Interpolation may also be viewed as temporal filtering. There are a number of schemes for k-space sampling and interpolation. Consider the case for which the k-space lines in sequential images are varied in a time interleaved manner such that the full k-space is periodically acquired. This is shown in Fig. 12.2, in which there is a case of twofold undersampling, with odd lines and even lines acquired on alternate frames. Interpolation methods, such as view sharing, or more general filtering, such as UNFOLD, may be used to reconstruct images with suppressed alias artefacts. For example, a view-shared reconstruction uses two sequential frames in a sliding-window fashion. View sharing may be described as a filter that provides temporal smoothing (see Discussion). The image frame rate is increased, although the effective temporal resolution is not improved. Interpolation errors which result from rapid changes will cause ghosting artefacts. The ghosting artefacts will “flicker” at the frame rate due to the sign changes caused by the interleaved acquisition order. The desired pixel and the ghost artefact which is temporally modulated effectively share the temporal bandwidth. The UNFOLD method exploits the property that the outer portion of the field of view is relatively static and uses a temporal filter with greater bandwidth for dynamic regions, realizing improved temporal resolution. The concept of bandwidth sharing is illustrated by means of temporal spectra (i.e., FFT of images series along

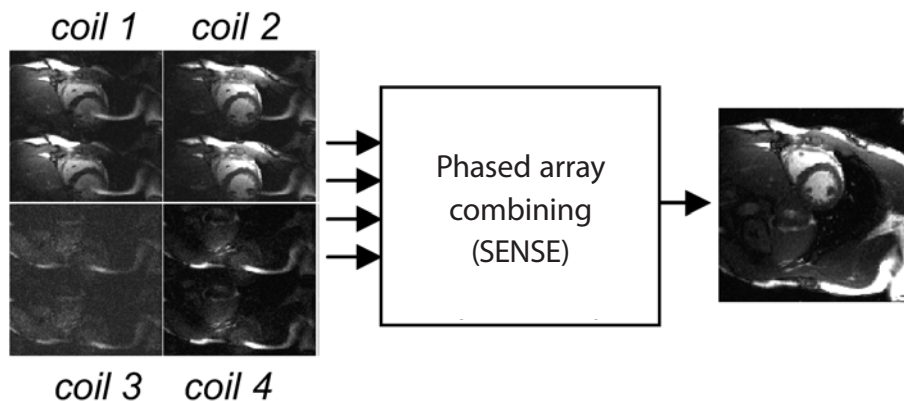


Fig. 12.1. Parallel imaging using SENSE method of phased-array combining

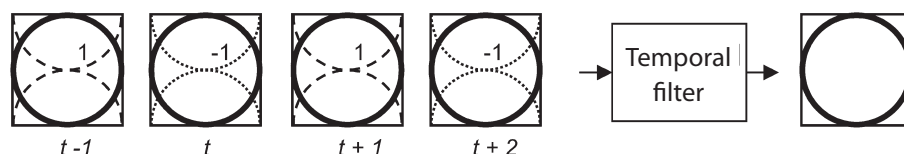


Fig. 12.2. Temporal filtering (interpolation) for suppression of reduced FOV alias artefacts

the time dimension) and is described more fully in the following paragraphs. Temporal filtering or interpolation may be equivalently implemented in the k-space domain providing the same effective bandwidth across the FOV, although this violates the strict bandwidth sharing formulation of the UNFOLD method.

12.1.3 Combined Spatial and Temporal Filtering

Parallel imaging and temporal filtering methods may be combined to achieve either higher acceleration factors or improved suppression of alias artefacts, and/or to realize auto-calibration of the parallel imaging combiner coefficients. The incorporation of temporal processing with image domain parallel imaging is referred to as TSENSE. Both parallel imaging and temporal filtering are linear operations and may be done in either order (commutative operations) as shown in Fig. 12.3. Figure 12.3a shows parallel imaging followed by temporal filtering, whereas Fig. 12.3b shows temporal filtering followed by parallel imaging; these are mathematically equivalent but will differ computationally. Figure 12.4 illustrates the case of auto-calibrating TSENSE, which may optionally include additional temporal filtering of the images. In the auto-calibrating scheme the temporal filter is typically a simple integration of multiple frames to provide a lower temporal resolution set of individual coil images with suppressed alias artefacts to compute the parallel-imaging coefficients.

Parallel imaging and temporal filtering may be combined to provide a higher acceleration factor, e.g., SENSE rate $2 \times$ UNFOLD rate 2, for a net TSENSE

acceleration of rate 4 (KELLMAN and McVEIGH 2000). In this case, coil sensitivities are estimated from separate reference data since the images may not be fully unfolded with a temporal filter for auto-calibration. Parallel imaging and temporal filtering may also be combined to provide a greater suppression of alias artefacts. For example, in the case of acceleration rate two aliased components are alternating phase; thus, the alias artefact is temporally frequency shifted to the band edge and may be suppressed by temporal low-pass filtering. The phase of the alias artefact does not alter the SENSE formulation; however, if the estimates of coil sensitivities are imperfect, there will be residual alias artefacts. Any residual artefact will be temporally frequency shifted to the band edge and thus may be further suppressed by temporal low-pass filtering. By combining both temporal and parallel imaging the resulting implementation achieves a high degree of alias artefact rejection with less stringent requirements on accuracy of coil sensitivity estimates and temporal low-pass filter selectivity than would be required using each method individually.

12.1.4 k-space Undersampling and Temporal Spectra

A number of schemes may be used for undersampling the acquisition of phase encodes in a time series of images. A few schemes are depicted in Fig. 12.5 which illustrate the acquisition of k-space vs time for four consecutive frames, with the solid line indicating phase-encoded lines that are acquired and the dashed lines indicating phase encodes that are skipped. Figure 12.6 illustrates an image with alias artefacts and associated temporal spectra for the cases corresponding to Fig. 12.5, where the bold lined circle portrays the desired object and the alias ghost artefacts are normal solid ($\pm\text{FOV}/4$) and dashed lines ($\text{FOV}/2$). Figure 12.5a and b are for the case of $R=2$ undersampling, and Fig. 12.5c and d are for $R=4$.

Figure 12.5a shows the static case of (conventional) undersampling with a fixed pattern, i.e., odd lines acquired at each time frame. In this case, the temporal spectra of the desired image and aliased artefacts are overlapping and must be separated with parallel imaging. Figure 12.5b shows the case of undersampling by 2, acquiring even and odd lines on alternate time frames. In this case, the alias ghost artefact (separated by $\text{FOV}/2$) has alternating polarity (± 1) and, therefore, is temporal frequency shifted to the band edge.

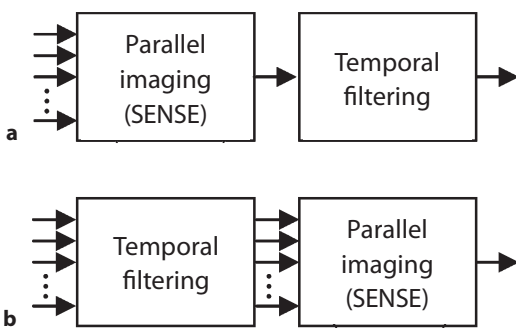


Fig. 12.3a,b. Combined parallel imaging with temporal filtering (TSENSE) implemented equivalently, as a parallel imaging then temporal filtering, or b temporal filtering then parallel imaging

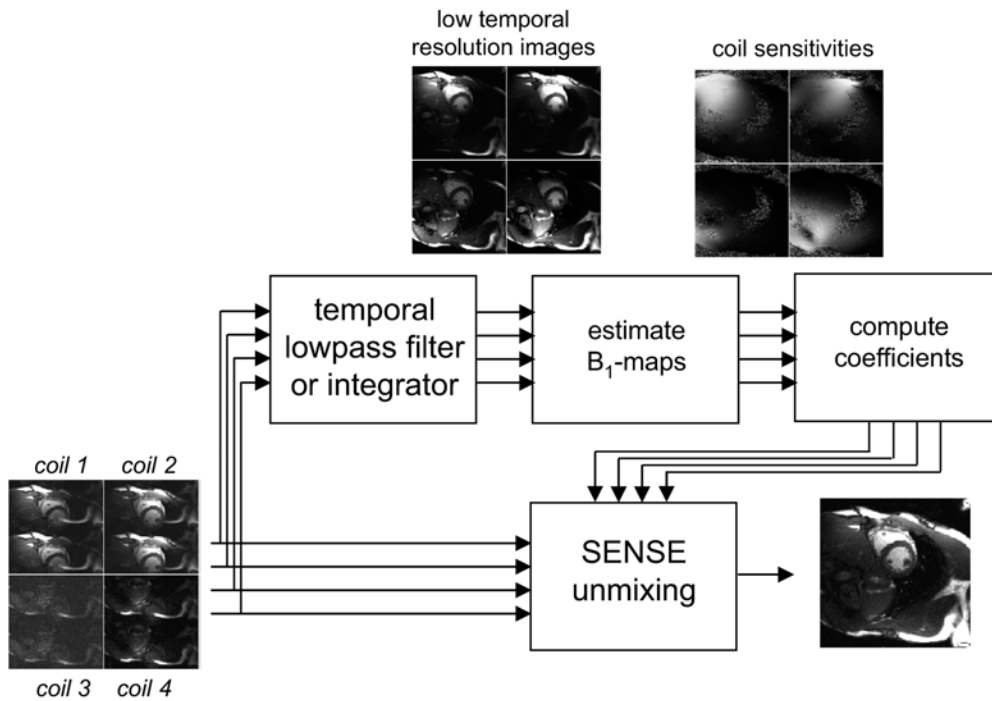


Fig. 12.4. TSENSE method for auto-calibrating parallel imaging

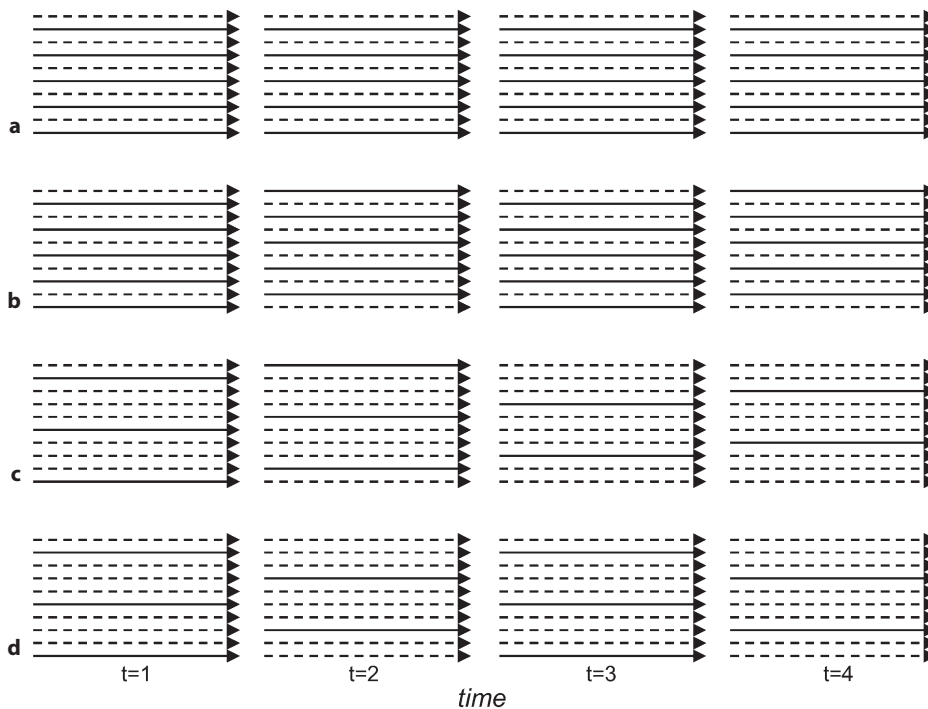


Fig. 12.5a–d. Various schemes for undersampled k-space acquisition. **a** Static phase encoding order ($R=2$); **b** odd–even phase encoding acquired on alternate time frames ($R=2$); **c** $R=4$ undersampled acquisition repeats every fourth frame (1,2,3,4, etc.); **d** $R=4$ undersampled acquisition repeats every other frame (1,3,1,3, etc.). *Solid lines* indicate phase-encoding lines that are acquired and *dashed lines* indicate phase encodes that are skipped.

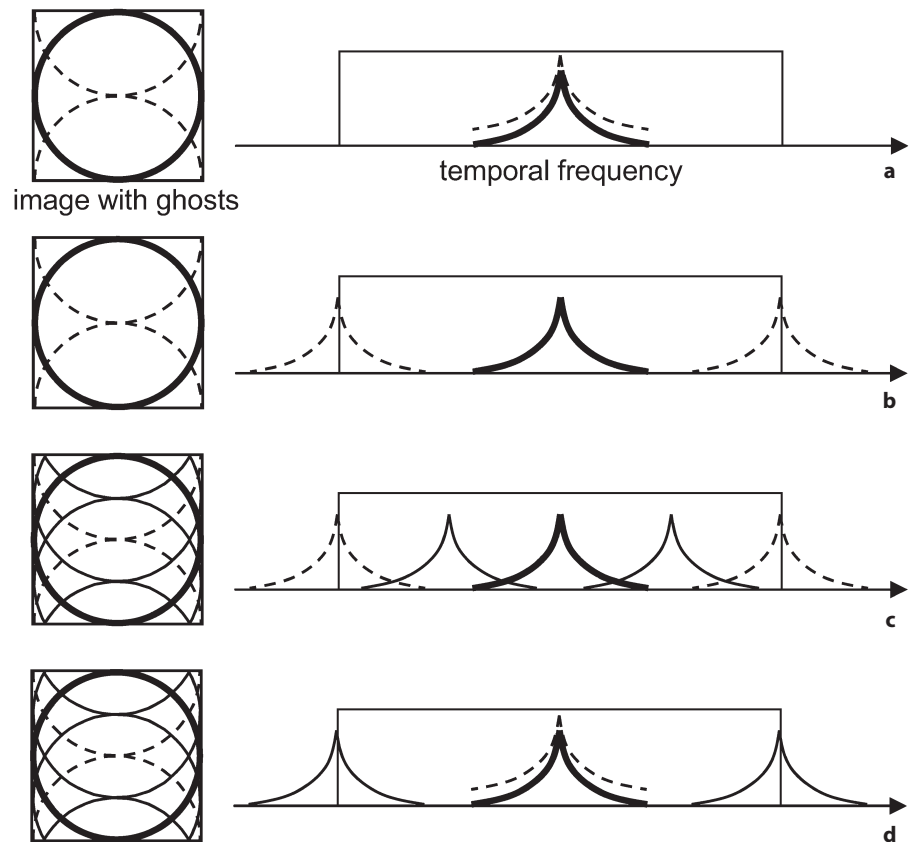


Fig. 12.6a-d. Temporal spectra and images with alias ghost artefacts illustrate the various undersampled k-space acquisition cases described in Fig. 12.5.

A real example of temporal spectra for the case of Fig. 12.6b is shown in Fig. 12.7, illustrating several methods. The raw signal (normal solid line) has desired component (center) and aliased artefact (band edge). The UNFOLD method was applied using a temporal filter with magnitude frequency response shown with dashed line. The UNFOLD filter passband was 90% of the available bandwidth causing only a slight decrease of the effective temporal resolution. The spectra for the UNFOLD signal (solid gray line) shows that while the band edge is suppressed, the band edge artefact had a wider temporal bandwidth (i.e., was not completely stationary) resulting in residual artefact. The spectra for parallel imaging using SENSE (dotted line) resulted in fairly good artefact suppression independent of temporal frequency; however, some residual artefact is evident at the band edge. The combination of SENSE and UNFOLD (bold solid line), which may be implemented by either approach of Fig. 12.3, resulting in a high level of artefact suppression. (Note that in the sampling scheme of Fig. 12.5b, full k-space is acquired every

$R=2$ frames, and the data may be integrated or low-pass filtered to derive a low temporal resolution set of individual coil images without artefacts, which may be used as an auto-calibrating reference as shown in Fig. 12.4.)

Figure 12.5c and d correspond to rate-4 acceleration using two different undersampling schemes which results in differences in the temporal spectra. In the case of Fig. 12.5c, the full k-space is acquired every $R=4$ frames (desired and alias spectra are distinct), and the data may also be used to derive an auto-calibrating references as previously described. The scheme of Fig. 12.5d does not acquire full k-space, and the spectrum for the FOV/2 alias artefact overlaps that of the desired image. This case does lend itself to the same auto-calibration method. Parallel imaging ($R=2$) may be used to suppress the FOV/2 artefact combined with temporal filtering ($R=2$) of the band edge to reconstruct images with net acceleration of rate $R=4$. This scheme uses parallel imaging to suppress the widely spaced ghost artefact (FOV/2) thereby improving the performance (SENSE g-factor). A number of other sampling

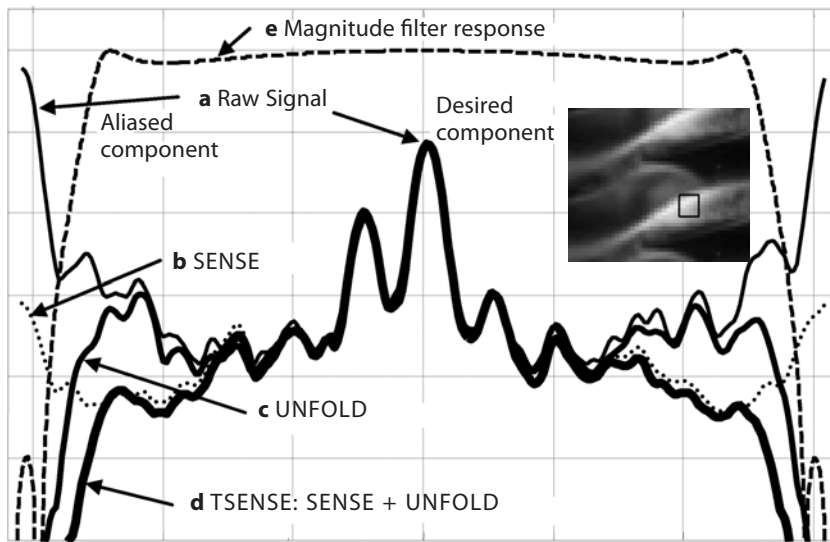


Fig. 12.7a–e. Average temporal spectrum of a region (*inset*) with both heart and aliased chest wall components. a Raw signal; b SENSE; c UNFOLD; d TSENSE; e temporal low-pass filter response

schemes are possible including variable density sampling (MADORE 2004).

12.1.5 2D TSENSE

In volume imaging applications using two phase-encoding dimensions (or spectroscopic imaging), it may be preferable to perform accelerated imaging in each of the two phase-encoded directions as shown in Fig. 12.8, rather than a higher rate along a single direction. This has been referred to as 2D SENSE (WEIGER et al. 2002). Depending on the specific coil sensitivity profiles and slice geometry, it may be possible to achieve a g-factor which is greatly reduced when compared with the same net acceleration along a single dimension. A sampling scheme for 2D TSENSE is shown in Fig. 12.9, corresponding to undersampling by rate 4 in the phase-encoding direction and by rate 3 in the partition-encoding direction.

12.2 Application Examples

The TSENSE may be used for a number of dynamic imaging applications. A few typical cardiac applications are presented as examples. The TENSE has also been applied in echo-planar imaging (EPI)-BOLD fMRI (DE ZWART et al. 2002).

12.2.1 Cardiac Segmented Cine 2D Imaging

Cardiac MR imaging is challenging due to the simultaneous need for moderately high resolution, ability to image during cardiac and respiratory motion, and relatively low SNR of imaging in the heart at the center of the torso. Parallel imaging offers a means of decreasing acquisition time which offers the user more flexibility to meet these challenges.

The cardiac short-axis images shown in Fig. 12.10 were acquired using the 32-channel Siemens 1.5-T Avanto and a prototype 32-element cardiac array (Invivo Corp). The array consisted of two 16-element 2D arrays with overlapping hexagonal elements with one array positioned on the chest, and the second array positioned on the back of the

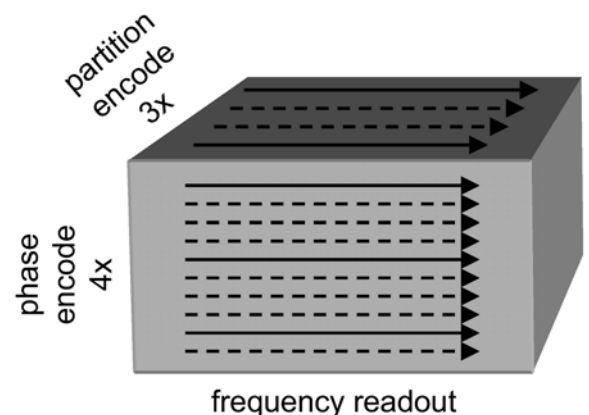


Fig. 12.8. k-space acquisition for 2D SENSE with under-sampling in both the phase and partition-encode directions.

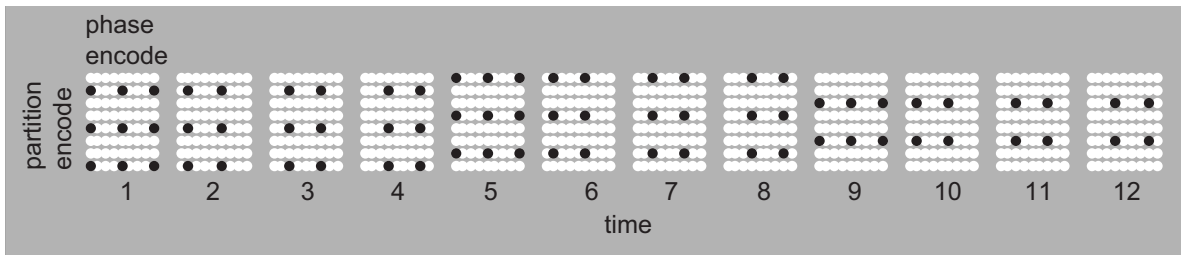


Fig. 12.9. k-space acquisition order for $R=4 \times 3=12$ 2D TSENSE example with under-sampling by four in the phase-encoding direction and undersampling by three in the partition-encoding direction. Complete k-space is acquired in $R=12$ phases.

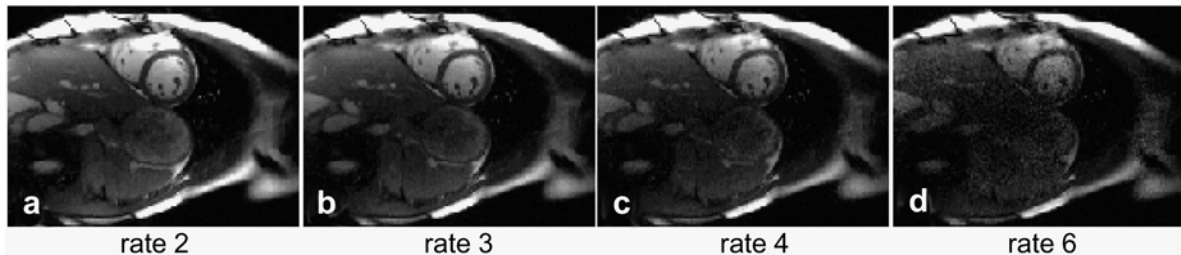


Fig. 12.10a–d. Short-axis cardiac cine images reconstructed using TSENSE at acceleration rates $R=2, 3, 4,$ and 6

patient. The coverage of the array was approximately 35 cm in the left–right direction and 30 cm in the superior–inferior direction. Cardiac imaging was performed using a breath-held, segmented, ECG triggered, true-FISP cine sequence. B_1 maps were calculated using the auto-calibrating TSENSE method. A single, doubly oblique, short-axis slice was acquired with phase encoding performed along the anteroposterior direction. Imaging parameters were matrix size= 192×108 , FOV= 320×240 mm², slice thickness=6 mm, readout flip angle= 50° , TE/TR= $1.41/2.82$ ms, views per segment=9, in-plane spatial resolution= 1.7×2.2 mm², and temporal resolution=25.4 ms. Breath-hold durations were 12, 6, 4, 3, and 2 heartbeats for acceleration at rates 1 (fully sampled), 2, 3, 4, and 6, respectively.

The quality of SENSE accelerated cardiac images at acceleration rates up to rate 4 was excellent using the 32-element array. Degradation was evident above rate 4 acceleration but may still be useful for some applications.

12.2.2 Real-Time Cardiac 2D Imaging

Patients with heart failure pose challenges for cardiac imaging due to increased difficulty with breathing and incidence of arrhythmias. Cardiac functional

imaging using breath-held, gated, segmented acquisition will frequently have artefacts, as shown in Fig. 12.11a for a patient with arrhythmia. Real-time, non-breath-held, non-ECG triggered imaging is possible with accelerated parallel imaging. An example of a real-time image for the same patient acquired using rate-4 TSENSE is shown in Fig. 12.11b.

Imaging was performed on a 1.5-T Siemens Avanto using an 8-element cardiac array (Nova Medical, Wilmington, Mass.). A true-FISP sequence was used with the following typical parameters: TE/TR= $1.4/2.8$ ms; 50° readout flip angle; and 6-mm slice thickness. The acquisition matrix was 192×80 with FOV= 300×250 mm² corresponding to an in-plane resolution of 1.6×3.1 mm², and a temporal resolution of 56 ms at rate $R=4$.

12.2.3 Contrast-Enhanced First-Pass Perfusion

Coverage of the entire heart during first-pass contrast-enhanced MRI with single-heartbeat temporal resolution is desirable for quantifying perfusion abnormalities. Multi-slice coverage may be achieved using saturation recovery with a relatively short preparation time (TI) and a gradient-echo (GRE) sequence with multi-shot EPI readout. Imaging quality may be improved at the expense of coverage by

increasing TI and readout flip angle. Parallel imaging may be applied to first-pass contrast-enhanced cardiac MR to yield greater spatial coverage for a fixed temporal resolution. Accelerated imaging also reduces the imaging duration per slice which reduces the possibility of motion blur. The saturation recovery time (TI) may be increased for improved contrast-to-noise ratio.

The TSENSE method (KELLMAN et al. 2001) was used to adaptively estimate B_1 maps using an interleaved phase-encoded acquisition order at acceleration rate $R=2$. The sequence timing is shown in Fig. 12.12 Odd and even phase-encoded lines were acquired on alternate heartbeats. The B_1 maps were calculated from a sliding window average of eight frames to reduce the sensitivity to breathing. No additional temporal filtering for further alias artefact suppression was applied to the TSENSE images.

Figure 12.13 shows example images of a single short-axis slice (of five acquired) during first-pass

perfusion with dipyridamole induced stress and at rest for a patient with a stress perfusion deficit in the inferior and lateral wall. The perfusion deficit in the stress study is clearly evident in Fig. 12.13d.

Imaging was performed on a 1.5-T Siemens Avanto using an 8-element cardiac array (Nova Medical, Wilmington, Mass.). A GRE-EPI sequence was used with the following typical parameters: 90° saturation recovery; echo-train length=4; TR=6.2 ms; 25° readout flip angle; 1600 Hz/pixel BW; and 8-mm slice thickness. The acquisition matrix was 128×80 with FOV=360×270 mm² corresponding to an in-plane resolution of 2.8×3.4 mm². The TI was 110 ms, where TI is defined at the center of k-space acquisition. The imaging window was 62 ms (142 ms per slice SR preparation time and overhead). Single heartbeat temporal resolution was accomplished with spatial coverage of five slices at heart rates up to 80 bpm with consistently good contrast and overall image quality.

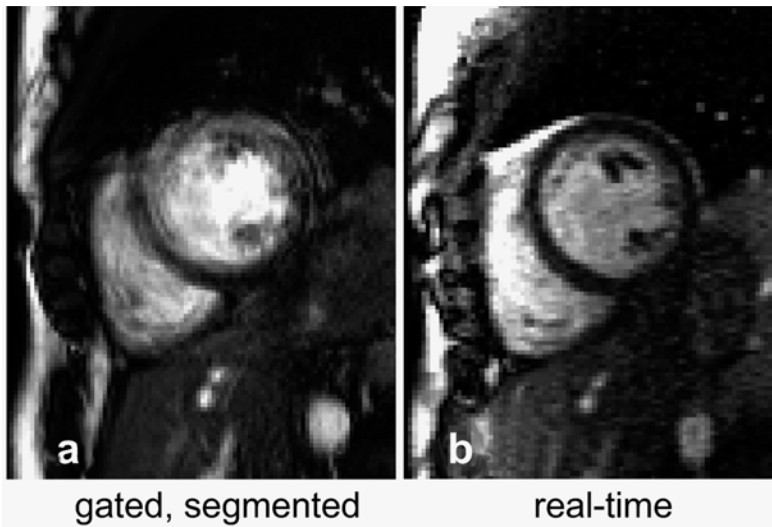


Fig. 12.11a,b. Short-axis cardiac cine image for a patient with arrhythmia for a conventional ECG-gated, segmented acquisition, and b real-time acquisition using TSENSE, non-ECG triggered

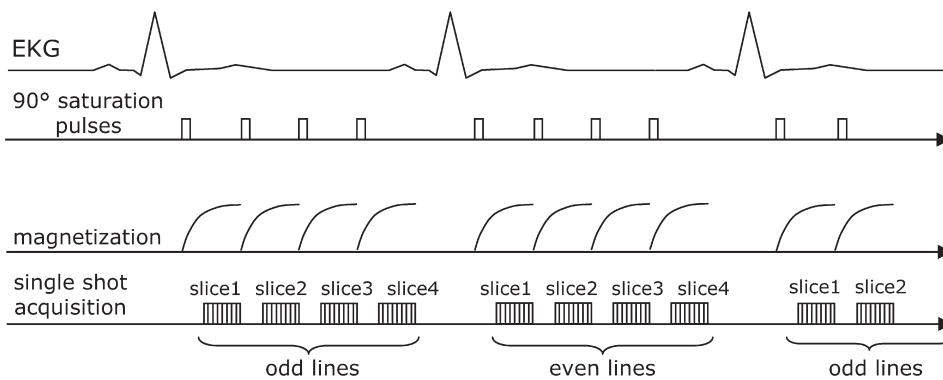


Fig. 12.12. Sequence timing for multislice first-pass contrast-enhanced perfusion with single-shot readout and single RR temporal resolution, acquiring even and odd phase-encoded lines on alternate heart beats for TSENSE reconstruction

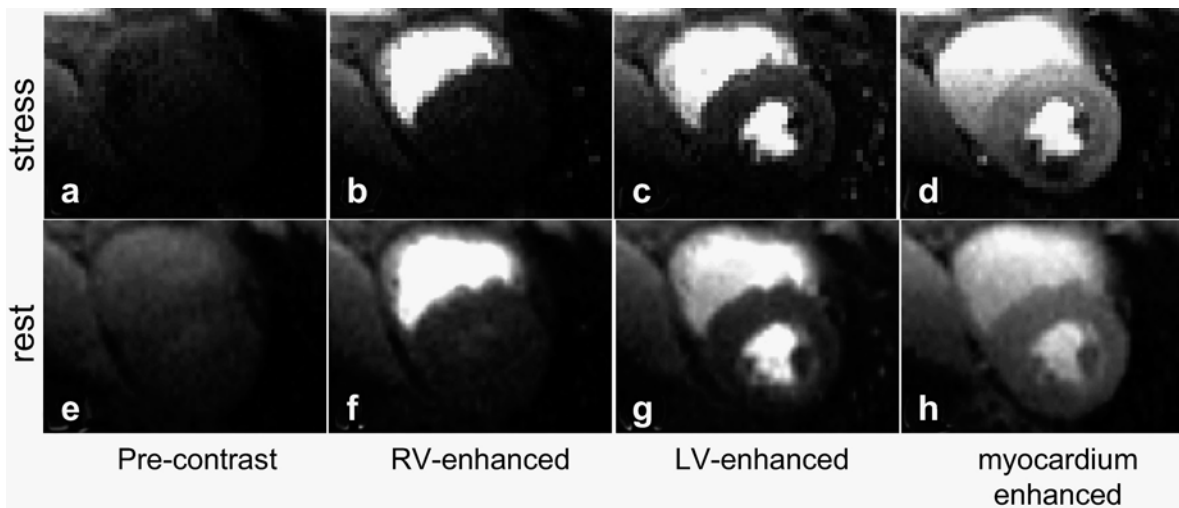


Fig. 12.13a–h. Example of first-pass contrast-enhanced perfusion images for patient with stress perfusion deficit in the inferior and lateral wall shown for single slice, acquired using GRE echo-planar sequence using rate-2 TSENSE. The *bottom row* is at rest and *top row* is with stress. a,e Pre-contrast; b,f RV enhanced; c,g LV enhanced; d,h myocardium enhanced

12.2.4 Cardiac Cine 3D Imaging

Cardiac cine 3D imaging offers the potential for full heart coverage in a single, segmented breath-held acquisition. A single acquisition eliminates breath-hold registration errors between slices that may occur in conventional 2D multislice imaging requiring multiple breath-holds. Parallel imaging using 2D SENSE (WEIGER et al. 2002) was used to reduce the breath-hold duration. A gated, segmented trueFISP sequence at acceleration rate $R=12$ was used to achieve spatial resolution of $1.8 \times 2.4 \times 7 \text{ mm}^3$ and approximately 30-ms temporal resolution within a single 18-heartbeat breath-hold.

Doubly oblique imaging was used with the partition encoding along the long axis of the heart. The phase-encoded and frequency-readout directions were in the short-axis plane with the frequency readout along the longer dimension of the body after in-plane rotation was applied. Encoding directions are shown in Fig. 12.14. The acquisition used rate $4 \times 3 = 12$ undersampling, with rate-4 undersampling in the phase-encoded dimension and rate-3 undersampling in the partition-encoded direction. The B_1 maps were estimated using the auto-calibrating TSENSE method. The k-space undersampling varied cyclically with complete k-space acquired in $R=12$ phases. The complete data set was integrated to reconstruct B_1 maps for calculating SENSE unmix-

ing coefficients. Since it is important to have artefact-free in vivo reference images for B_1 map estimates, approximately 25% slice oversampling was used in the partition-encoded dimension to reduce wrap. The acquisition matrix was $192 \times 108 \times 18$ with four slices discarded after reconstruction. Example images for rate $4 \times 3 = 12$ are shown in Fig. 12.15 for a normal volunteer subject. The example shown used a FOV of $340 \times 255 \times 98 \text{ mm}^3$ providing a spatial resolution of $1.8 \times 2.4 \times 7 \text{ mm}^3$. At rate $4 \times 3 = 12$, the actual number of lines acquired were $108/4 = 27$ phase encodes $\times 18/3 = 6$ partition encodes. The sequence parameters were: bandwidth = 1400 Hz/pixel; TR = 3.08 ms; and 50° readout flip angle. There were nine views per segment providing $9 \times 3.08 = 27.7$ ms temporal resolution. The total breath-hold duration was $(108/4) \times (18/3) / 9 = 18$ heart beats. Imaging was performed on a 32-channel Siemens Avanto 1.5 T scanner using a prototype 32-element cardiac phased array (Invivo Corp).

The measured g-factor values for which 95% of the pixels in the heart region fall below were 5.2 for rate $4 \times 3 = 12$ and 2.9 for rate $4 \times 2 = 8$. Despite a relatively high g-factor, the SNR and artefact suppression were quite good using 3D imaging.

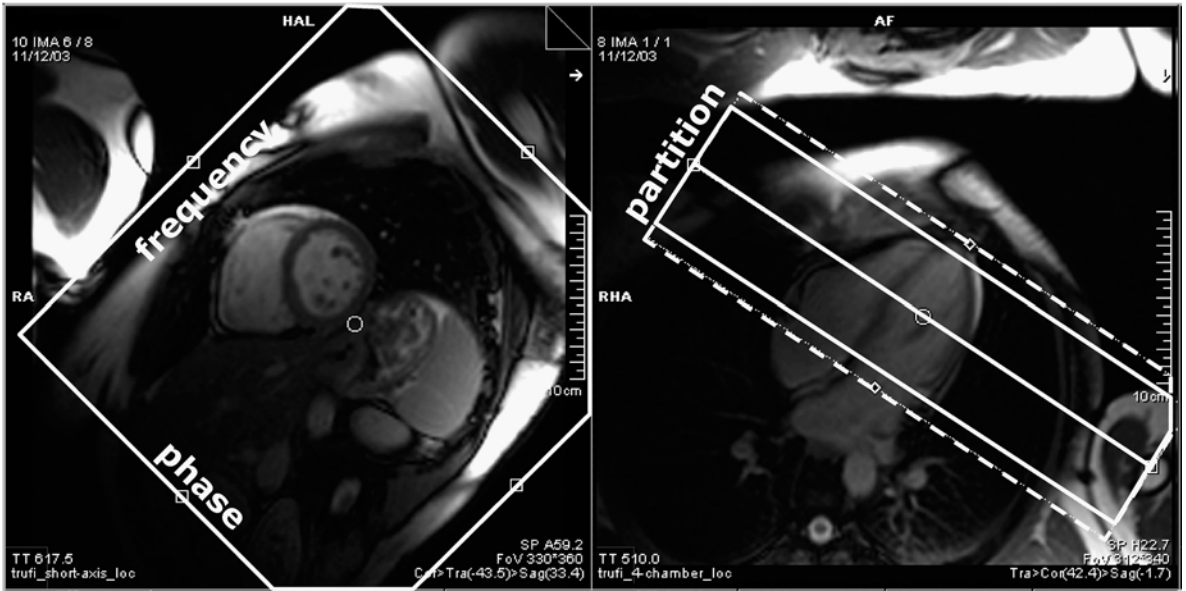


Fig. 12.14. Graphic prescription for cine 3D doubly oblique imaging. The partition encoding is along the long axis of the heart. The phase-encoded and frequency-readout directions were in the short-axis plane with the frequency readout along the longer dimension of the body after in-plane rotation was applied.

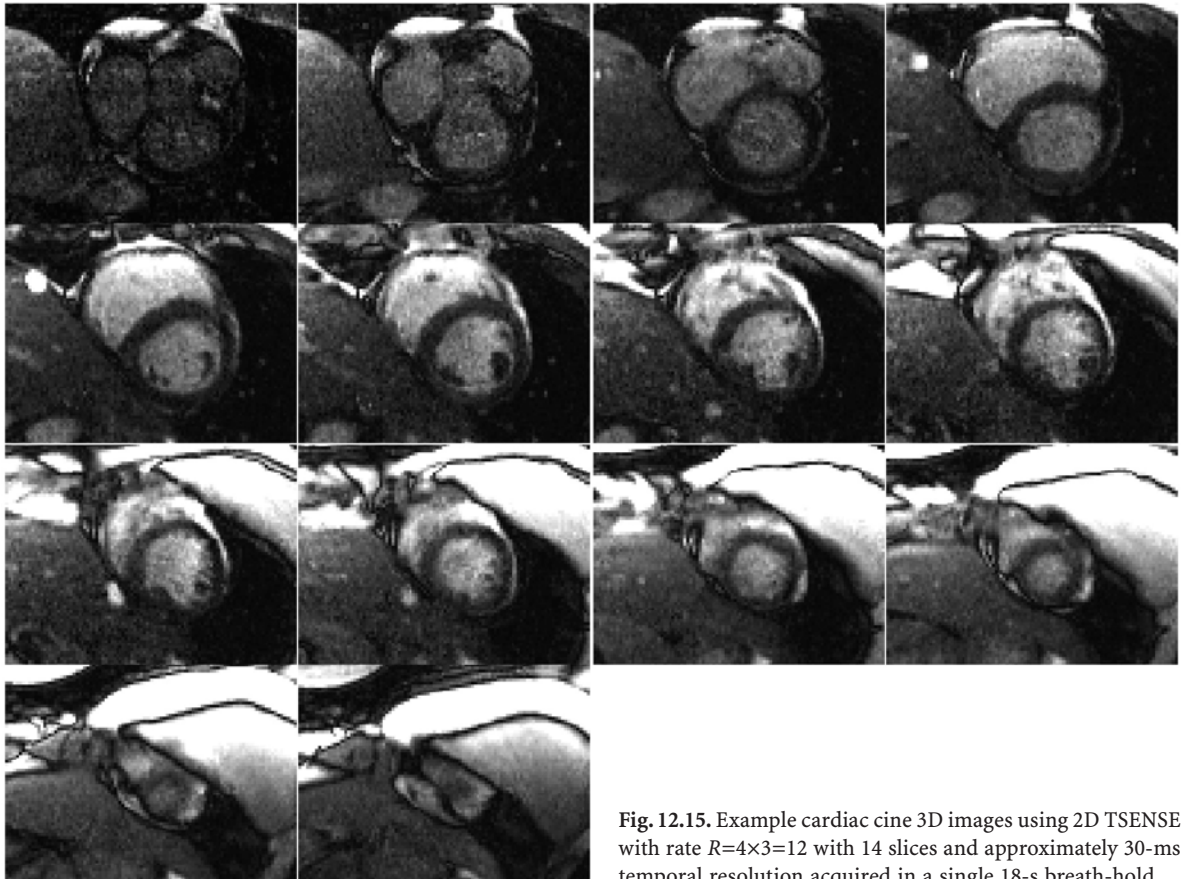


Fig. 12.15. Example cardiac cine 3D images using 2D TSENSE with rate $R=4 \times 3=12$ with 14 slices and approximately 30-ms temporal resolution acquired in a single 18-s breath-hold

12.3

Discussion

Parallel imaging provides accelerated imaging with a wide temporal bandwidth. A number of methods, such as view sharing, produce temporally interpolated images at a higher frame rate; however, the effective temporal resolution is not improved. In order to place view sharing and more general temporal filtering (e.g., UNFOLD) in the same context, Fig. 12.16 illustrates the equivalence between k-space and image domain temporal filtering. In this diagram, the undersampled acquisition matrix has been zero-filled for missing data at each time frame. After temporal filtering, the missing k-space is filled with temporally interpolated values. In the case of simple view sharing which combines even and odd k-space data for each frame, the temporal filter is a sliding

window filter which is applied to each k-space value after zero-filling (e.g., even, 0, even, 0, even ... or 0, odd, 0, odd,...). Equivalently, in the image domain, the FOV/2 artefacts are alternating sign (± 1) and a sliding window filter at each pixel will cancel the alias artefact provided that it is stationary. The simple sliding window used in view-shared reconstruction is a crude low-pass filter which zeros the band edge with greatest artefact but does not improve the temporal resolution. Improved temporal filters which interpolate using additional time frames provide a flatter temporal frequency response, although they will have a correspondingly increased transient response which may cause intensity fluctuations (filter ringing). The filter may be implemented directly in the time domain as a weighted sum or equivalently using FFT-based filtering (at each pixel).

Temporal filtering (interpolation) methods rely on the tissue corresponding to aliased artefacts being sta-

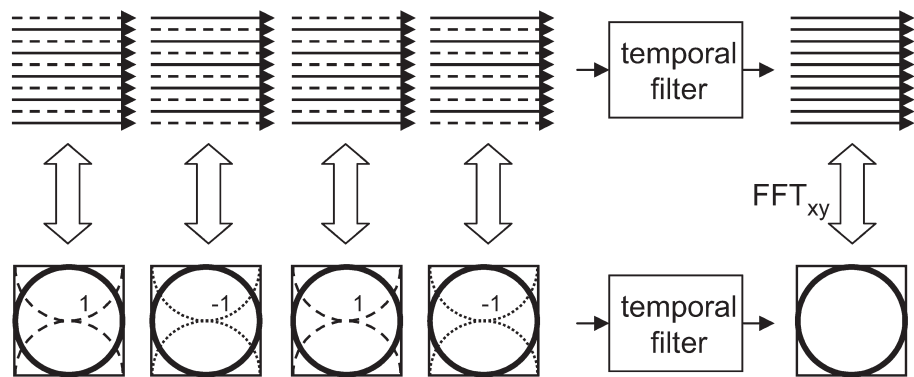


Fig. 12.16. Equivalence of k-space and image domain temporal filtering implementations

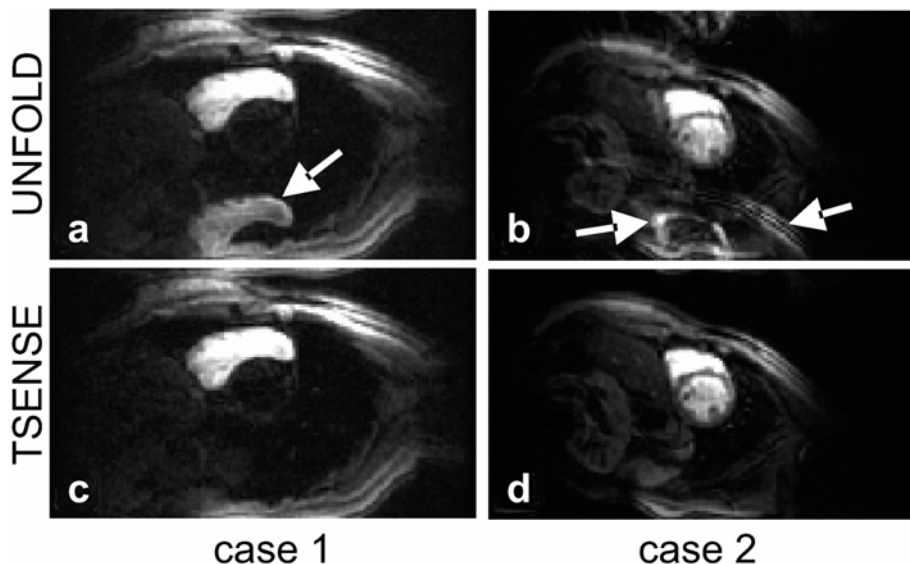


Fig. 12.17a–d. Residual artefacts in UNFOLD reconstruction due to dynamic signal fluctuation. Arrows in a indicate artefact due to rapid signal enhancement of RV blood pool and in b due to respiratory motion of chest wall

tionary with constant or slowly varying signal intensity. The extent that the tissue intensity is changing, there will be residual artefacts as illustrated in Fig. 12.17. In case 1 (left column), a first-pass contrast enhanced cardiac perfusion image is shown after UNFOLD filter reconstruction (Fig. 12.17a), for a time point where the right ventricle (RV) is enhancing. The rapid change in signal intensity due to contrast enhancement leads to a residual artefact of the RV displaced by FOV/2. The TSENSE reconstruction (Fig. 12.17c) of the same time frame using combined spatial and temporal filtering provides artefact suppression despite the rapid change. A second example in Fig. 12.17b and d shows a chest wall artefact due to respiratory motion in the UNFOLD reconstruction of Fig. 12.17b which is suppressed using TSENSE in Fig. 12.17d.

References

- Breuer FA, Kellman P, Griswold MA et al. (2005) Dynamic autocalibrated parallel imaging using temporal GRAPPA (TGRAPPA). *Magn Reson Med* 53:981–985
- d’Arcy JA, Collins DJ, Rowland IJ et al. (2002) Applications of sliding window reconstruction with cartesian sampling for dynamic contrast enhanced MRI. *NMR Biomed* 15:174–183
- Hu X, Parrish T (1994) Reduction of field of view for dynamic imaging. *Magn Reson Med* 31:691–694
- Kellman P, McVeigh ER (2000) Method for combining UNFOLD with SENSE or SMASH. *Proc Eighth Scientific Meeting. Int Soc Magn Reson Med* 1507
- Kellman P, McVeigh ER (2001) Ghost artefact cancellation using phased array processing. *Magn Reson Med* 46:335–343
- Kellman P, Epstein FH, McVeigh ER (2001) Adaptive sensitivity encoding incorporating temporal filtering (TSENSE). *Magn Reson Med* 45:846–852
- Kellman P, McVeigh ER (2006) Phased array ghost elimination. *NMR Biomed.* 19:352–361
- Kostler H, Sandstede JJ, Lipke C et al. (2003) Auto-SENSE perfusion imaging of the whole human heart. *J Magn Reson Imaging* 18:702–708
- Madore B (2002) Using UNFOLD to remove artefacts in parallel imaging and in partial-Fourier imaging. *Magn Reson Med* 48:493–501
- Madore B (2004) UNFOLD-SENSE: a parallel MRI method with self-calibration and artefact suppression. *Magn Reson Med* 52:310–320
- Madore B, Glover GH, Pelc NJ (1999) Unaliasing by Fourier encoding the overlaps using the temporal dimension (UNFOLD), applied to cardiac imaging and fMRI. *Magn Reson Med* 42:813–828
- Nezafat R, Kellman P, Derbyshire JA, McVeigh ER (2005) Real Time Blood Flow Imaging using Auto-Calibrated Spiral Sensitivity Encoding. *Magn Reson Med.* 54:1557–1561
- Pruessmann KP, Weiger M, Scheidegger MB et al. (1999) SENSE: sensitivity encoding for fast MRI. *Magn Reson Med* 42:952–96.
- Sodickson DK, Manning W (1997) Simultaneous acquisition of spatial harmonics (SMASH): fast imaging with radiofrequency coil arrays. *Magn Reson Med* 38:591–603
- Tsao J, Boesiger P, Pruessmann KP (2003) k-t BLAST and k-t SENSE: dynamic MRI with high frame rate exploiting spatiotemporal correlations. *Magn Reson Med* 50:1031–1042
- Weiger M, Pruessmann KP, Boesiger P (2002) 2D SENSE for faster 3D MRI. *MAGMA* 14:10–19
- Zwart JA de, van Gelderen P, Kellman P et al. (2002) Application of sensitivity-encoded EPI for BOLD functional brain imaging. *Magn Reson Med* 48:1011–1020